Final Draft
of the original manuscript:

MECHANICAL BEHAVIOUR OF DISSIMILAR FRICTION STIR WELDED TAILOR WELDED BLANKS IN Al-Mg ALLOYS FOR MARINE APPLICATIONS

E. E. Feistauer[a](*), L. A. Bergmann[b], L. S. Barreto[a], J.F. dos Santos[b]

[a] Federal University of Sergipe, Department of Material Science and Engineering Av. Marechan Rondon s/n, 49100-000 São Cristovão, Sergipe, Brazil.
[b] Helmholtz-Zentrum Geesthacht, Institute of Materials Research, Materials Mechanics, Solid-State Joining Processes, Max-Planck-Str. 1, 21502 Geesthacht, Germany.
(*) *Email:* eduardo.feistauer@hzg.de

Abstract

Tailor welded blanks (TWB) in Al alloys are an attractive structural solution for application in the shipbuilding sector, mainly due to reductions in weight and lower production costs. In the present study, the global and local mechanical properties of dissimilar friction stir welded TWB were assessed. The joints were manufactured with dissimilar Al-Mg alloys and thicknesses (6 and 8 mm) of particular interest to the shipbuilding sector (AA5083 and AA5059). A digital image correlation system (DIC) linked to a tensile test system was used to characterise the local strain fields, and true stress-strain curves were generated for several TWB sub-zones. Microhardness and DIC analyses showed that the stir zone of the TWB presented overmatching in relation to the weakest base material, and that the joints displayed excellent overall mechanical performance that was comparable to the AA5059 base material in terms of strength and ductility. The fatigue strength was evaluated by means of tension-tension fatigue tests, and the TWB joints reached the fatigue keen with a stress range of 70MPa.

Keywords: Tailor-welded blanks, friction stir welding, Global and local mechanical properties, Digital image correlation system.

1. Introduction

The shipbuilding sector, as well as all modern transportation industries, is faced with demands for greater productivity while at the same time ensuring the manufacture of consistently high quality products, reducing levels of re-working, saving energy, and minimizing operational costs. Furthermore, it is imperative that new designs and all the stages of production comply with stringent environmental regulation. Within this context, the application of Friction Stir Welding (FSW) as a manufacturing process to weld Tailor Welded Blanks (TWB) for Al structures can contribute to the development of high speed craft and lightweight ships that are more fuel efficient [1].

Assemblies in TWB were first introduced by the automotive industry as a procedure to improve productivity and promote efficient usage of materials. This concept consists of welding blanks made of different materials with the same or varying thicknesses, prior to forming. The main advantages of TWB in the automotive sector are related to better control of the flow and distribution of materials during the stamping process, combined with improved structural weight distributions. The possibility of optimizing the weight of the welded structure, coupled with cost reduction, has raised the attention of other transportation sectors such as aerospace and shipbuilding. Despite the attractive advantages of the TWB concept, the high performance aluminium alloys employed in the transportation sector present carefully created microstructures, and the high temperatures encountered during conventional fusion welding can harm mechanical performance of the joints [2]. Thus, alternative solid state welding technologies that offer lower process temperatures (below the melting temperature), such as FSW, have been recently developed by the scientific community for welding tailor-welded blanks.

The process feasibility of AA7075-T6 blanks in seven different thickness combinations (between 3mm and 5mm) was investigated by Fratini et al [3,4] using finite element (FE) analysis and experimental validation. They highlighted the influence of process parameters, tool geometry, and the double tool inclination angle on the production of sounds TWB joints. Zadpoor et al. [5,6] evaluated FSW joints produced with dissimilar aluminium alloys (AA2024-T3 and 7075-T6) and thicknesses (in the range 2-2.5mm). The global and local mechanical properties were assessed in quasi-static tests, and the microstructural features were characterized. However, the majority of the published studies on this topic have focused on FSW process optimization for thin blanks (1.0-2.6 mm) with an emphasis on automotive applications [7–10]. Meanwhile, in even the lightest ships, the robust structure means that high stiffness sheets must be employed to ensure structural safety. It is therefore necessary to develop and evaluate TWB made of thicker sheets. Another gap of knowledge in the literature is related to the long-term degradation and fatigue behaviour of aluminium alloys in TWB configurations welded by FSW. This information is indispensable for industrial application of these materials as structural components. Garware et al. [11] investigated the quasi-static tensile and tension-tension fatigue behaviour in TWB composed of AA5754 with thicknesses combination of 1.06 and 1.66mm and pointed out the high fatigue strength of the TWB joints produced by FSW. It was found that the fatigue failure occurred on the thin gauge side and originated from the tool marks left on the weld surface.

Due to the geometrical features of TWB, as well as, the particular microstructural features resulting from the process and the asymmetric temperature flow during FSW, TWB joints exhibit highly heterogeneous mechanical properties. The local mechanical properties needed to understand the inhomogeneous constitutive properties of FSW joints can be assessed by specific characterisation techniques. These include micro and nanohardness testing, testing of miniature specimens extracted from different weld regions, testing of thermally simulated materials, and digital image correlations (DIC) as described by Reynolds and Duvall [12]. Each method has its advantages and disadvantages, and the main limitations of these techniques are related to the accurate assessment of the plastic behaviour of the welds (hardness test) and difficulties associated with producing and testing miniature specimens. In the case of DIC, the complete monitoring of plastic behaviour is limited by the strength of the weakest partner of the joint [12–14]. Despite its limitations, the DIC methodology has been successfully used to assess local stress-strain curves and describe heterogeneous properties of FSW welds, considering local thickness variations [13], as well as in shear testing[15].

In this article, the heterogeneous mechanical behaviour of TWB joints welded by FSW was evaluated using quasi-static and cyclic loading, and the observed microstructural features were analysed. The TWB joints were manufactured by FSW using dissimilar alloys and thicknesses (6 and 8mm) of particular interest in the shipbuilding sector (AA5083 and AA5059). A brief evaluation of local constitutive properties in different regions through the TWB joint was performed by digital image correlation linked to the tensile test system.

2. Experimental procedure

2.1 Production of welded samples

The dissimilar base materials consisted of cold rolled AA5083 (8mm) and AA5059 (6mm) aluminium alloy plates measuring 200mm (width) by 1000mm (length). The standard chemical compositions [16] and those obtained by in-house analysis are presented in Table 1. The friction stir welded TWB were produced in a single run, and the FSW tool geometry consisted of a threaded conical pin, with three flats (8mm diameter) and a spiral (scroll) shoulder with a diameter of 20mm. The process parameters and the tool geometry are provided in Table 2. Due to asymmetric temperature fields and the massive plastic deformation, typical of the FSW process [17], the thicker plate (AA5083) was placed on the advancing side of the weld, with the purpose of submitting this sheet to higher temperature in order to facilitate the softening and mixing of the whole material

volume in the weld portion. In order to compensate for the different thicknesses of the two blanks, a second tool inclination angle of 5.7° was applied in the direction of the thinner plate (Fig 1). The concept of a double angle for TWB has been introduced by HZG [18,19].

Table 1: Chemical compositions of the aluminium alloys

	Weight %	Si	Fe	Cu	Mn	Mg	Cr	Zn	Ti
AA5083	Standard[16]	<0.4	<0.4	<0.1	0.4-1	4-4.9	0.05-0.25	<0.25	<0.15
	Test result	0.118	0,306	0,073	0,550	4,89	0,073	0,126	0,011
AA5059	Standard[16]	<0.45	<0.5	<0.25	0.6-1.2	5-6	<0.25	0.4-0,9	<0.2
	Test result	0.048	0.107	0.013	0.920	5.56	<0.01	0.640	0.020

Table 2: Welding parameters

n [RPM]	F_a [kN]	v [mm/s]	A [°Grad]	Tool geometry	
				Ø Shoulder	Ø Probe
600	25	6	1	20	8

n = Rotational speed, F_a = Axial force , v = Welding speed, A = Tilt Angle
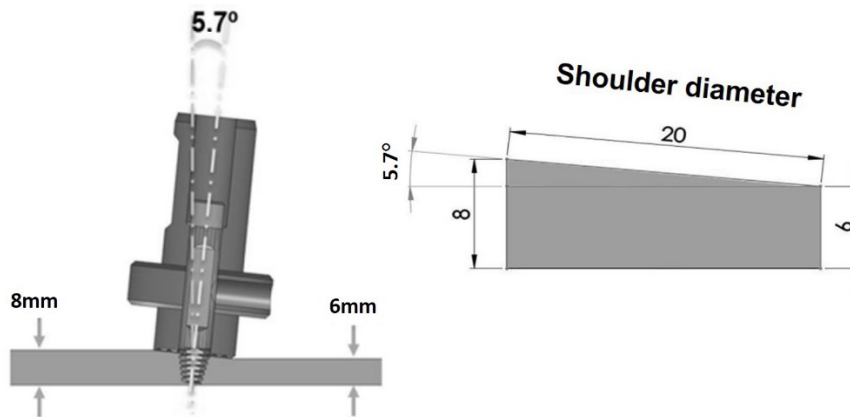

Figure 1: Tool sketch and detail of the side tilt angle.

2.2 Macro and microstructure characterization

Macroscopic examination test samples were cut from the welds and mounted, ground, and polished up to 0.05μm colloidal silica suspension. The microstructure was revealed by electrochemical etching using Baker's reagent. An optical microscope with 90° polarized light and a digital camera was used to capture the microstructure of the cross-section samples. The fracture surfaces of the tensile test and fatigue samples were characterized by scanning electron microscopy (SEM) using a Quanta[TM] 650 FEG microscope with beam energy of 15kV and magnification of up to x10000.

2.3 Assessment of mechanical properties

The mechanical properties of the TWB samples were evaluated at local and global scales. The local changes in mechanical properties across the welded TWB joint were firstly determined by

micro-hardness testing. The micro-indentations were performed using 0.2 kgf load applied for 10 seconds, according to the ASTM: E384 standard, using a Zwick/Roell ZHV micro-hardness machine, equipped with a hardness measuring head and a fully automated x/y-table. Two micro-indentation profiles with 40mm length were obtained over the transverse section samples, with the stir zone placed at the centre. The first profile was performed 2mm below the surface edge of the thinner sheet, and the second was shifted vertically 2mm from the first profile. The distance between indentations was 0.5mm.

The global mechanical properties of the TWB were evaluated using quasi-static and cyclic loading tests. Within the framework of quasi-static loading, tensile tests were carried out according to the ASTM: E8M standard, using a Zwick/Roell universal testing machine with a load capacity of 200 kN. The tests were performed at room temperature, with constant crosshead speed of 1mm/min. The displacement was recorded by an MTS extensometer (gauge length of 75mm). A GOM digital image correlation system (DIC) linked to the tensile test machine was used to assess the local strain behaviour. During the measurement, trigger signals were sent every second to a 4-MP camera (50 mm focal length). Management of the entire measurement, evaluation, and documentation procedure was accomplished with the integrated ARAMIS software.

In terms of cyclic loading, fatigue tests were performed to evaluate the fatigue endurance limit of the TWB joints. These tests were performed using a servo-hydraulic fatigue test machine, in accordance with ASTM: E466. In total, 21 specimens were tested under pure cyclic tension load until final failure. A sine wave-form with frequency of 10 Hz and stress ratio of 0.1 was employed in all cases. The fatigue endurance limit was defined as a stress level below which no fatigue failure would occur after $6x10^6$ cycles. The results of the fatigue testing were statistically analysed as recommended by ASTM: E739.

3. Results and discussion

3.1 Microstructure

The heat generated during the FSW process is strongly influenced by two factors: the friction between the tool and the work-piece, and plastic deformation [17]. It is well known that FSW generates asymmetric temperature fields, and also that there are two additional factors that accentuate this phenomenon: namely the heat capacities of the different base materials and the vortex velocity field [17,20]. As a result, there are significant variations in the microstructures of friction stir welds in dissimilar TWB joints. The macrographic analysis of such a joint shows a full penetration weld and absence of defects (Fig. 2). Moreover, it can also be observed that the welding process dramatically altered the central portion of the weld (the stir zone, SZ), which has been completely replaced by a fine-grained, equiaxed recrystallized microstructure (Figs. 2(b) and 2(f)). Evidence of material flow can also be observed in this region. Adjacent to the SZ, (left of the cross-section) it is possible to identify the thermo-mechanically affected zone (TMAZ) corresponding to the advancing side (AS), (Fig. 2 (g)), which has severely deformed grains towards the plastic flow direction.

On the opposite side of the SZ, on the retreating side (RS) (Fig. 2 (e)), grains with distorted shapes can also be observed due to the severe deformation applied during the FSW process. Since the AS of the weld is affected to a greater extent by the vortex velocity, the microstructure variations from the SZ to the TMAZ were more drastic, leading to a more well-defined border at the AS, compared to the RS. The base materials exhibited typical microstructures of cold rolled Al alloys, with grains that were elongated in the rolling direction. The microstructural changes described above for a dissimilar TWB joint are typical of Al-Mg alloys welded by FSW, and have been described in more detail in the literature [21,22].
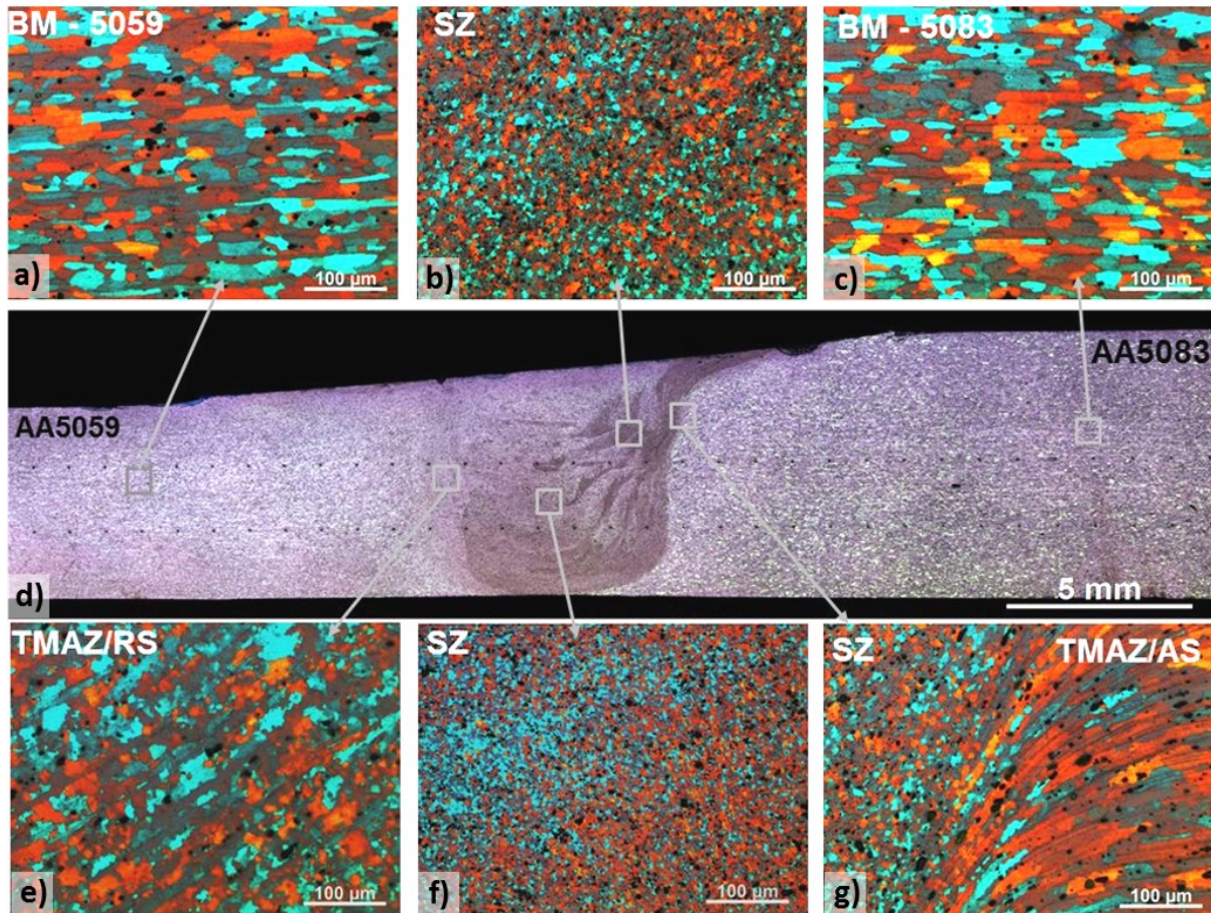
Figure 2: Macrograph and microstructure of a friction stir welded TWB joint in dissimilar AA5059/AA5083 configuration: (a) microstructure of AA5059 base material, (b) stir zone, (c) AA5083 base material, (d) joint macrograph, (e) TMAZ at the joint retreating side, (f) SZ, and (g) TMAZ at the advancing side of the joint.

3.2 Microhardness profile

Due to the microstructural changes caused by the FSW process, the mechanical properties of the joints exhibited substantial heterogeneity. The local mechanical properties assessed by Vickers microhardness, measured along a transverse section of the TWB joint (Fig. 3), showed an asymmetric hardness profile, which was primarily caused by the microstructural differences between the two base materials (94HV and 87HV for AA5059 and AA5083, respectively). In the central portion of the weld, indicated in the hardness plot by the shoulder contact area (Fig. 3), there was an increase in the microhardness value. This could be explained by microstructural changes, such as the formation of dynamic recrystallized grains that had greater grain surface and edge per unit of volume, as well as increased dislocation density in this region [20–22]. The maximum value reached in the SZ was 102HV. Between the SZ and the TMAZ in the AS, the microhardness values continuously decreased to close to that of AA5083. This can be explained by the increasing participation of the AA5083 alloy in the stir zone.
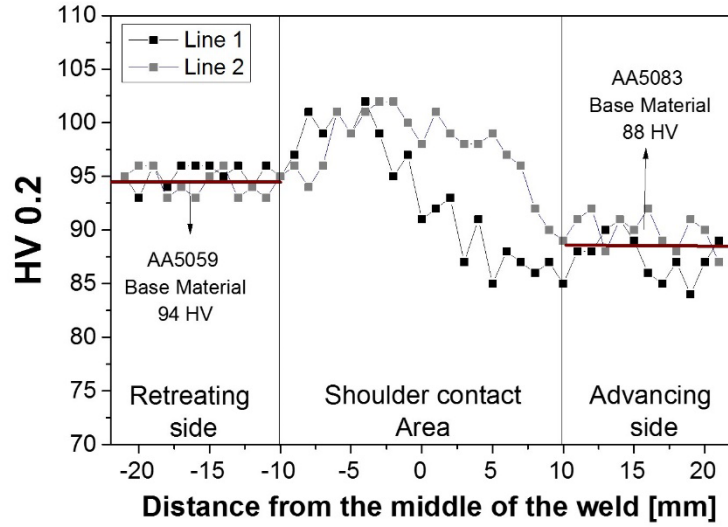
5

Figure 3: Hardness profile on the TWB joint.

3.3 Tensile Tests

Since the welds were made with two dissimilar alloys and sheets with different thicknesses, the overall plastic deformation behaviour of the joints was substantially heterogeneous. A preliminary estimation of whether both sheets underwent plastic deformation under monotonic loading, or whether the plastic deformation was concentrated only in the thin sheet, was made by applying the Limiting Strength Ratio criterion (LSR) [23,24]. A TWB joint satisfies this criterion when the thick sheet strain reaches the yield strength (σ_y) and on the other hand, the thin sheet strains reach the ultimate strength (σ_T), and is given by:

$$\sigma_{T_b} . t_b = \sigma_{y_a} . t_a \Rightarrow LSR = \left(\frac{\sigma_{y_b}}{\sigma_{T_a}}\right) = \frac{t_b}{t_a} \tag{1}$$

This criterion proposes that when the thickness ratio (t_b/t_a) of two sheets forming a TWB does not exceed value (σ_{yb}/σ_{Ta}) under quasi-static loading, the sheet with greater thickness undergoes plastic deformation perpendicular to the weld line. When the opposite occurs, the thickness ratio is greater than the LSR, the plastic deformation is concentrated on the thinner sheet perpendicular on the weld line, and the thicker material does not reach its yield point [23,24]. The TWB configuration investigated in the present study, with a thickness combination of 6 and 8mm, presented a strength ratio value of 0.58, which was less than thickness ratio (0.75) (Table 3). It can therefore be assumed that during the tensile test both sheets underwent plastic deformation.

Table 3: Limiting Strength Ratio calculation

Thickness combination	6.0 - 8.0mm
t_b/t_a	0.75
σ_{yb}/σ_{Ta}	0.58

Fig. 4(a) presents engineering stress-strain curves for three welded specimens extracted from the same TWB joint. The specimens failed on the thinner base metal (AA5059), and showed satisfactory mechanical properties when compared to the base material (Table 4). The stress-strain curves almost overlap each other, giving a clear indication of the high reproducibility of the process. Since in the TWB configuration the cross-sectional area along the gauge length varies, due to the thickness gap (6mm to 8mm), a conservative approach was adopted to calculate the tensile

6

properties, taking into account the cross-sectional area of the thinner plate (120mm^2). The serrated yielding that appears on the TWB joint stress-strain curve (the Portevin-Le Chatelier effect) is described in detail in the literature [25,26].

The deformation behaviour of the TWB during tensile testing was monitored by DIC. The strain maps obtained for the TWB are presented in Fig. 4(b). The results clearly showed that the strain was heterogeneously distributed across the specimen, mainly due to the stress concentration factor of TWB joints as well as microstructural changes in the weld zone, as previously discussed. All the specimens were tested in as-welded condition, the FSW process results in a very smooth and gradual thickness transition. As a consequence, a lower stress concentration factor is generated in the transition line, displacing the strain evenly to the thinner sheet, as shown in the strain map obtained after 900 seconds (Fig 4(b)).
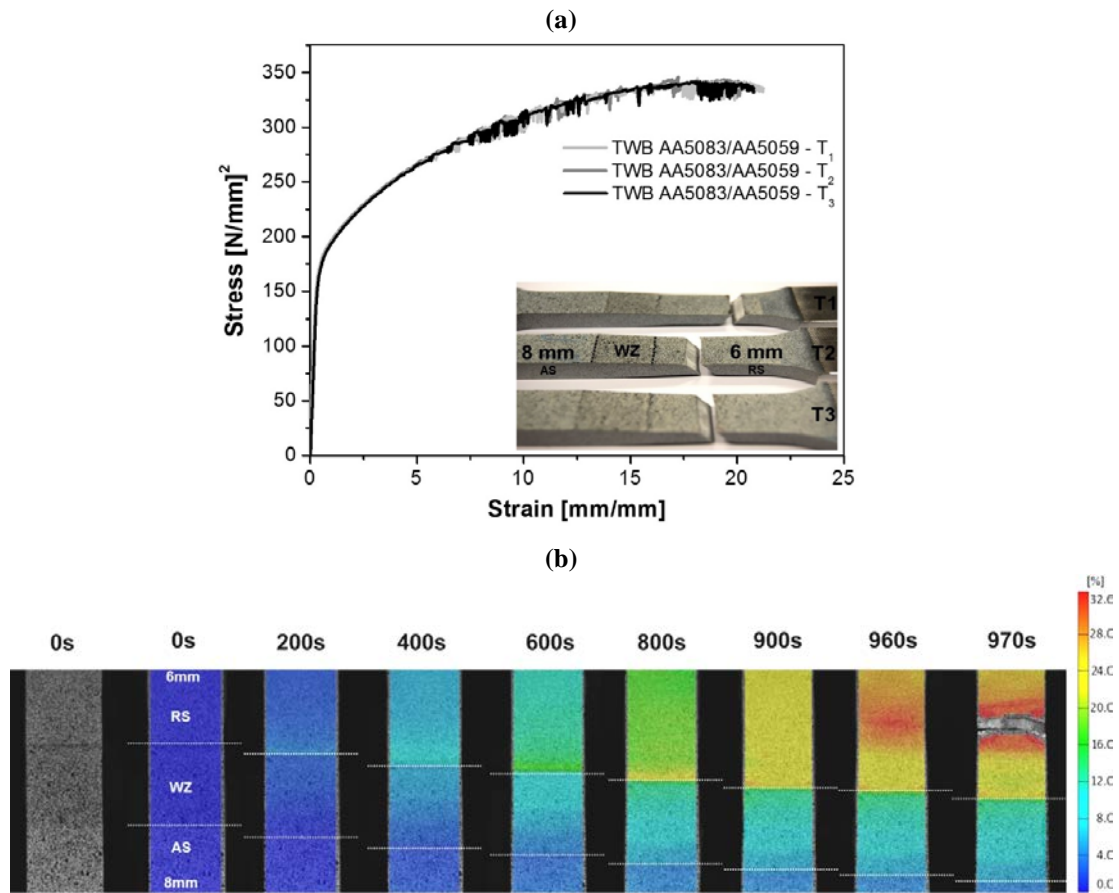
(a)

(b)

Figure 4: Tensile stress-strain curve for the TWB joint (a) and strain maps resulting from the DIC measurement (b). A typical speckled black pattern contrast applied over the white painted surface of the transverse specimen used for DIC measurement is shown in the image at 0s.

Table 3: Mechanical properties of the TWB AA5083/AA5059 weld.

	TWB Al5083/Al5059	AA5083 8mm thickness		AA 5059 6mm thickness	
		RD	PRD	RD	PRD
Rp0.2 [MPa]	195.5 ± 0.7	161.5 ± 1.9	161.7 ± 1.2	207.4 ± 1.6	141.1 ± 2.2
UTS [MPa]	343.9 ± 1.8	330.3 ± 2.1	326.0 ± 0.5	368.4 ± 0.8	310.9 ± 5.4
A [%]	20.9 ± 0.3	16.5 ± 2.5	20.4 ± 1.4	20.6 ± 1.7	22.4 ± 0.9

RD = Rolling direction; PRD = Perpendicular to the rolling direction

3.4 Local mechanical properties assessed by DIC

Using the DIC technique, the strain coordinates are determined only on the specimen surface, and information perpendicular to the surface is missing. Hence, it is not possible to calculate a complete strain tensor [27]. The stress fields were determined assuming that the lack of information in the thickness direction was not significant and by applying a simple procedure that took into account local thickness variations in the region under evaluation. A similar approach was used by Leitão [13] to derive stress-strain curves using DIC, and is necessary because the iso-stress condition is not fulfilled when testing TWB samples, due to the thickness variation. Thus, knowing the local strain values through all load stages during the tensile test (Fig. 5(a)), the local reduction of area in the zone under study during a determined load stage can be estimated by the following equation:

$$A^i = A_0^i exp(-\varepsilon^i) \qquad (2)$$

Where A^i_o is the initial cross-sectional area of the tensile specimen in the evaluation zone and ε^i corresponds to the local axial strain matched by DIC. By dividing the applied load, recorded at exact time that the DIC system measured the strain, by the corrected cross-sectional area (A^i) the stress spread along the TWB joint can be calculated. A linear area increment path was used to describe the thickness variation through the weld line in accordance with the measurements from the cross-section macrographs.

The stress concentration diagram computed by this methodology is shown in Fig. 5(b). Each diagram line corresponds to a single load stage computed through a section that vertically crosses the region of analysis, as shown in the strain map in Fig. 5(a). The stress concentration is highest in the thinner sheet away from the weld centre, where the highest values of major strain were measured, as previously discussed. The stress spread along the joint decreases linearly with the gradually increase of the thickness. By accumulating the stress values of each diagram line at a particular point located across the vertical line shown in the strain map, and knowing the corresponding strain values, presented in Fig. 5(a), it is possible to create a local stress-strain curve for any specific weld region.

In order to evaluate the accuracy of this procedure, engineering stress-strain curves were computed for the two base materials. The results are presented in Fig. 6, where curves generated for a region approximately 30mm away from the weld centre (plotted as solid squares) are compared against the stress-strain curves obtained by testing for the base materials (specimens extracted in the rolling direction and perpendicular to the rolling direction, grey solid lines). It can be observed that the local stress-strain curves obtained by DIC for the thinner AA5059 base material are in good agreement with the curves obtained by standard test. For the thicker AA5083 base material, the DIC curve almost exactly tracked the base material curve (Fig. 6(b)). Since the anisotropic mechanical properties were less pronounced for AA5083 than for AA5059, the DIC curves computed for the AA5083 base material showed satisfactory agreement for the rolling direction as well as perpendicular to the rolling direction.
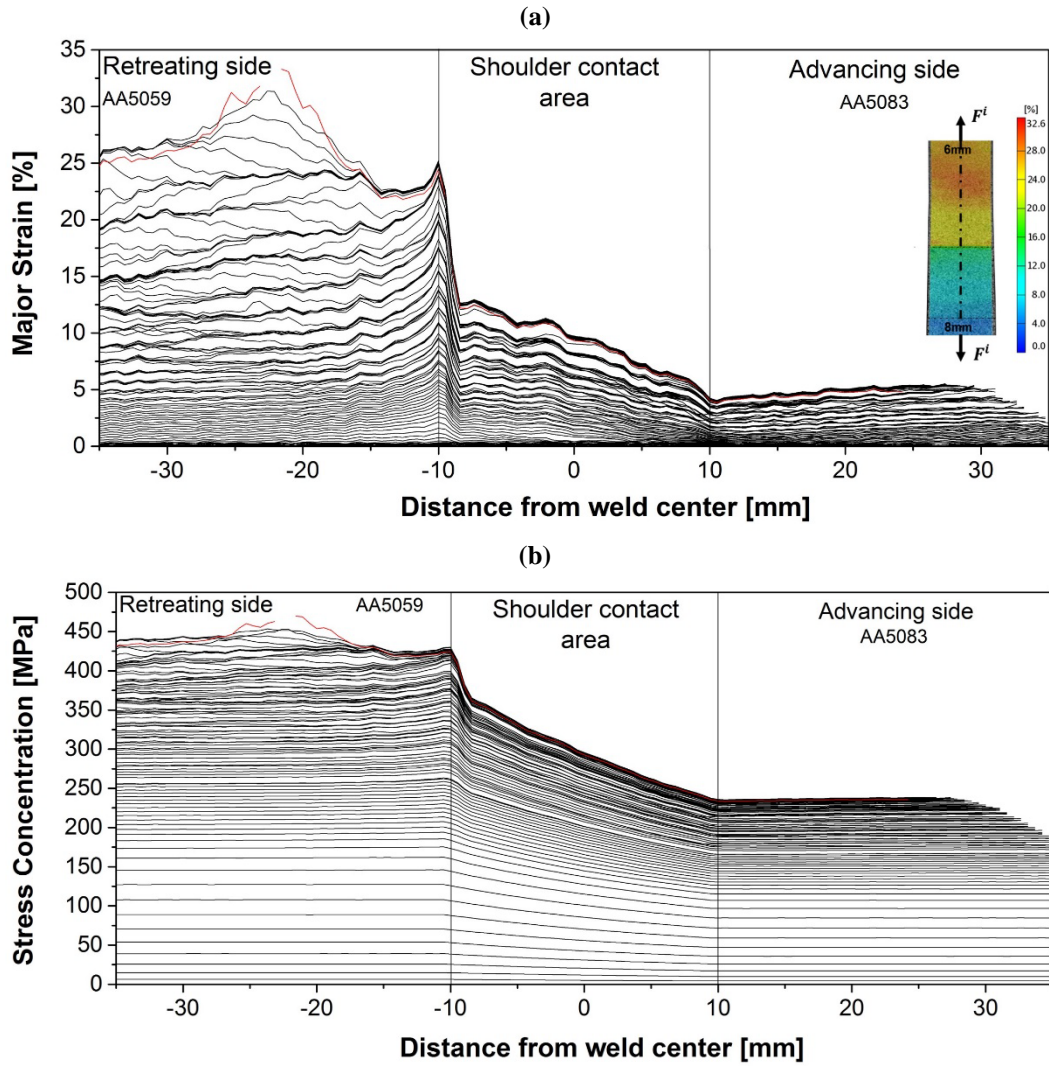
(a)

(b)

Figure 5: (a) Major strain of a section through all load stages; (b) stress concentration diagram computed by correlation of the major strain with the load applied in the tensile test
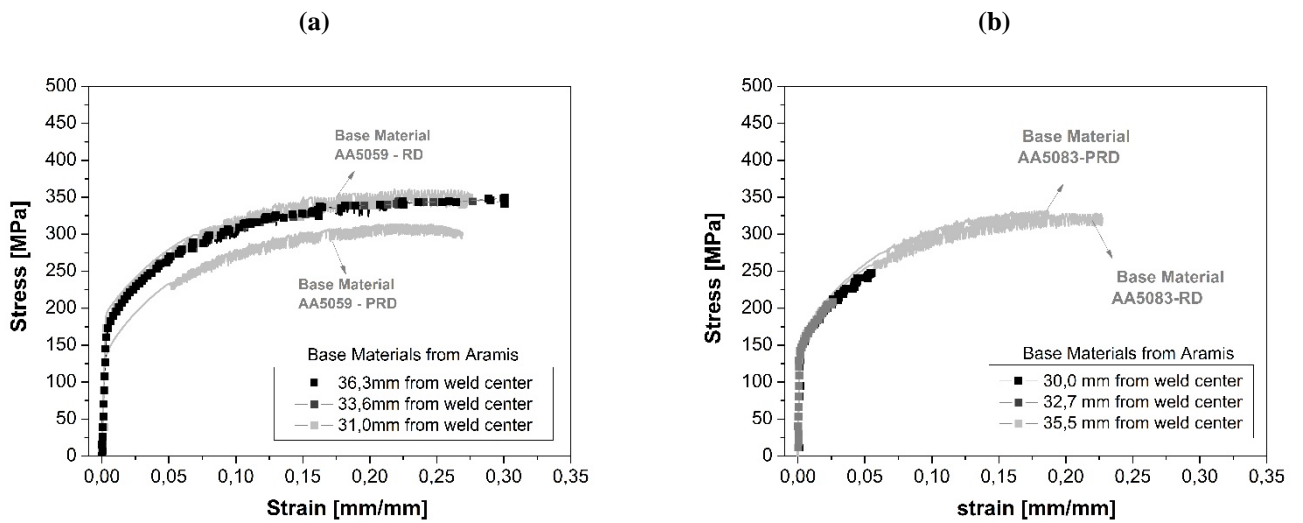
(a)

(b)

Figure 6: (a) Stress-strain curves for AA5059 base metal, perpendicular (PRD) and parallel (RD) to the rolling direction, and TWB joints compared to the base material curves computed from the DIC data; (b) the same comparison for the AA5083 base metal.

The results discussed above (Fig. 6) showed that the methodology adopted to evaluate the DIC results was valid and could satisfactorily be used to analyse local properties in TWB. In other words, stress-strain curves of any individual weld zone could be generated in order to understand changes in local mechanical properties, as shown in Fig. 7. Based on the microstructural analysis of a TWB joint, seven zones were identified (see section 3.1 and also Fig. 7). The cut-off point for the true stress-strain curves was defined by the weakest point of the joints, located at 23.2mm from the weld centre in the 6mm sheet. The plastic strain decreased towards the thicker sheet however, it is important to note that the stress concentration levels in the thicker sheet (AA5083) visibly exceeded the yield strength, confirming the LRS prediction.
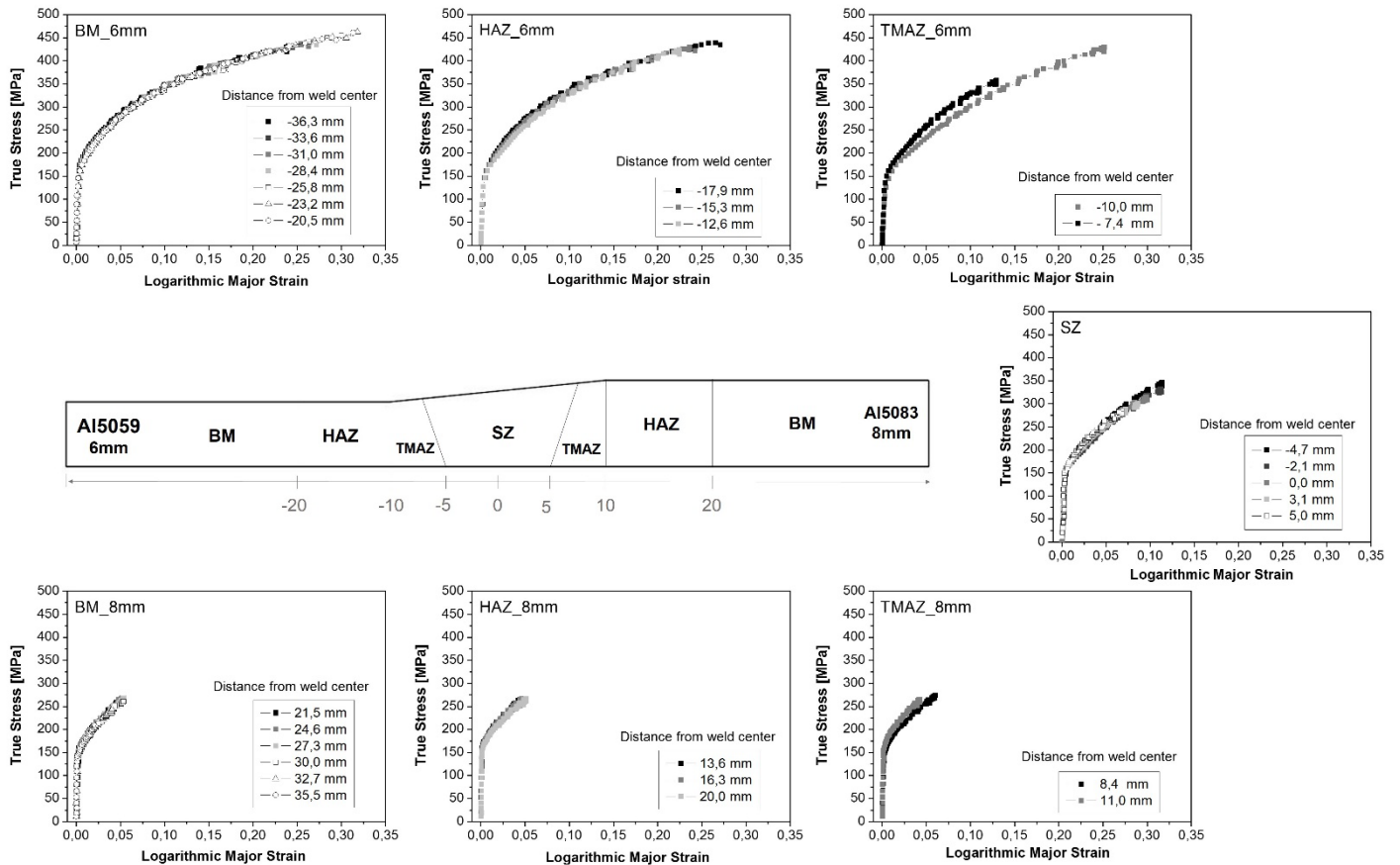

Figure 7: Local stress-strain curves computed by DIC for specific microstructural regions through the TWB joint.

The results of the microhardness tests (Fig. 3) provided a clear indication of the heterogeneity of the local mechanical properties. To substantiate these results, the yield and tensile stresses at a true strain value of 2% were calculated by projecting a line parallel to the linear elastic portion of the curves, with strain offset points at 0.002 and 0.02, respectively, across the TWB joint (Fig. 8). The calculated average yield strengths were approximately 155MPa for AA5083 and 182MPa for AA5059. These values were comparable to the yield strengths obtained in standard tensile tests (Table. 4). The average yield strength in the SZ (between -5 and 5mm) tended to increase relative to the AA5083 placed at the AS, in agreement with the hardness profile results, and the value lay between those for the two base materials, at approximately 161MPa. This can be explained by the effect of mixing with a higher strength alloy (AA5059), and also by recrystallization phenomena in the SZ. Due to mismatch of mechanical properties and geometric characteristics in TWB joints, local constraints can impose premature strain, which could have occurred in the HAZ of the 6mm thickness sheet (located at -10mm from the weld centre). Such a phenomenon may be caused by the adjacent harder material in the SZ, as well as the thickness increase in this region, resulting in a yield strength curve decrease to values close to 140MPa in the RS of the joint. This effect, as well as the

local mechanical properties at the 0.002 strain offset, tended to be reproduced at higher strain levels, as shown in the true strain curve at 2% (Fig. 8).
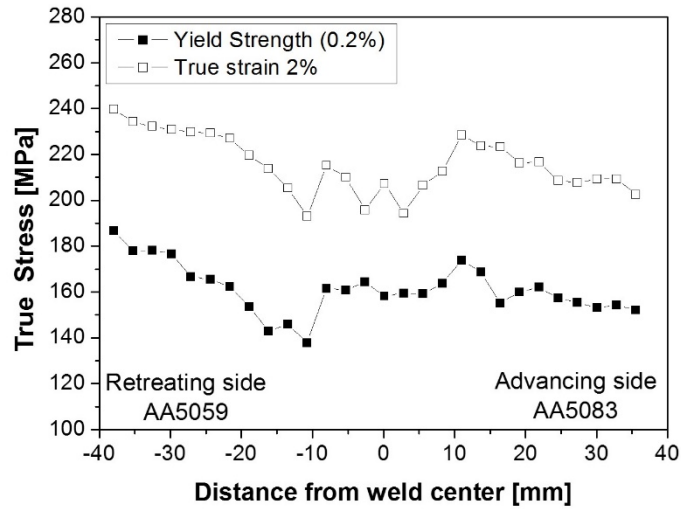

Figure 8: Tensile properties obtained by DIC across the TWB joint.

3.5 Fatigue test

Fig. 9(a) presents the S-N curve obtained for the TWB. The complete test parameters for each specimen tested are listed in Table 5. The assessment of fatigue data is usually based on a nominal stress range (σ_{max} - σ_{min}) [28]. The maximum and minimum stresses were calculated taking into account the cross-sectional area of the thinner sheet, as previously discussed in section 3.3. The S-N curve is identified by the characteristic fatigue strength of the detail in MPa at 2 million cycles as recommended by IIW for fatigue design of welded joints and components [28]. This value is the fatigue class (FAT). The estimated fatigue strength for the TWB taking into account the 95% confidence interval was 56MPa. The TWB specimens reached the fatigue limit at a maximum load of 78MPa, as a result of which failure was not observed for three specimens during fatigue tests at this load level. The mean curve equation, shown in Fig. 9(a), displayed a steeper slope (m = 4.2) compared to S-N curves for welded joints (m = 3). This effect was because the high stress amplitude tests were performed with 100% of the yield strength of the TWB. The high stress amplitude values caused the mean curve to tilt slightly towards higher slope values.

It is well known that fatigue crack initiation is a highly surface-sensitive phenomenon, and since the TWB specimens were tested in an as-welded condition, the surface instability produced by the shoulder marks on the weld line provided favourable crack initiation sites. Due to the stress concentration factor resulting from the change in cross-section along the weld line, crack initiation took place in the retreating side of the TWB joint, over the shoulder marks. The fracture surfaces typical of each load condition are illustrated in Fig. 9(b). The observed morphological features were typical of fatigue-tested specimens. Multiple crack initiation sites could be identified in specimens where the load applied was equivalent to 100% of the yield strength.
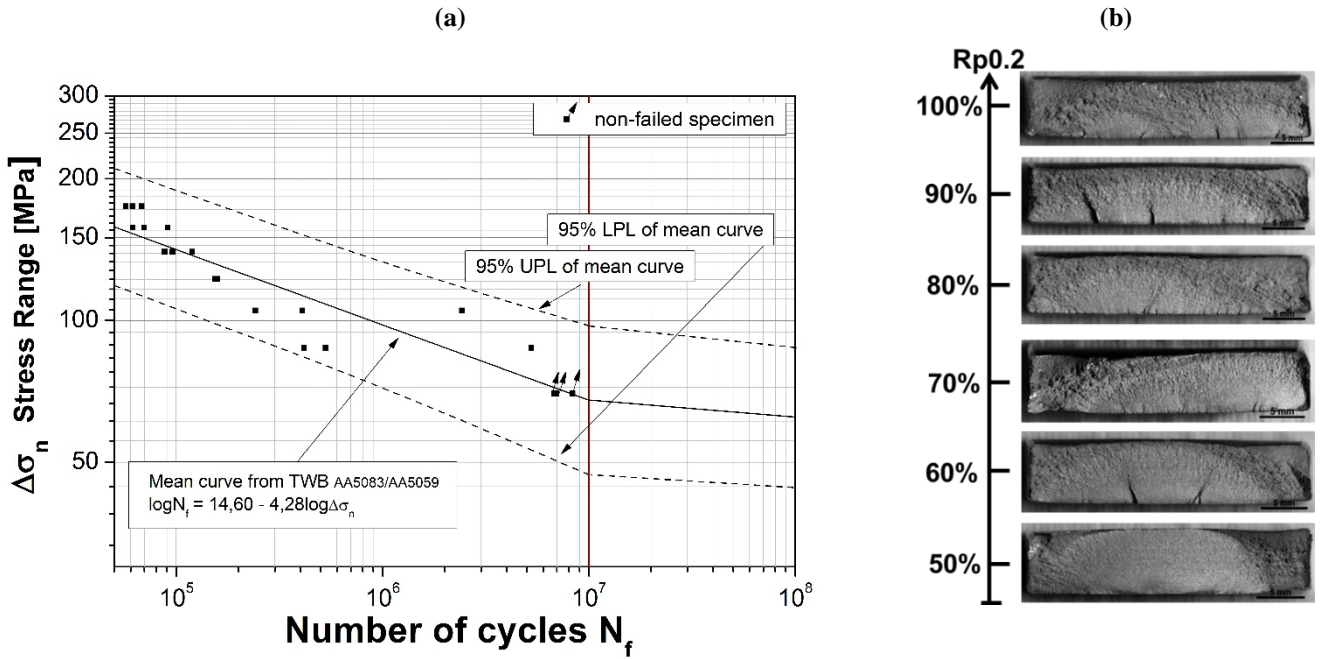
11

Figure 9: S-N curve for the TWB joint (a) and fatigue fracture surface detail for each load condition tested in relation to the yield strength of the TWB joint (b).

Table 4: Fatigue experimental data

Samples	Load %	F_{max} [N]	F_{min} [N]	Mean [N]	Ampl [N]	$\sigma_{máx}$ [MPa]	σ_{min} [MPa]	$\Delta\sigma$ [MPa]	Ampl [MPa]	Cycles
R1										61209
R2	100	35010	3501	19256	15755	195	19	176	88	56850
R3										67987
R1										61511
R2	90	31509	3151	17330	14179	175	18	157	79	90689
R3										69736
R1										119510
R2	80	28008	2801	15404	12604	156	16	140	70	95666
R3										87633
R1										153931
R2	70	24507	2451	13479	11028	136	14	122	61	154497
R3										158192
R1										241466
R2	60	21006	2101	11553	9453	117	12	105	53	407671
R3										2423015
R1										528847
R2	50	17505	1751	9628	7877	97	10	87	44	5239323
R3										415858
R1										8328712
R2	40	14004	1400	7702	6302	78	8	70	35	6970733
R3										6766684

3.6 Fracture surfaces

The fracture surfaces of specimens submitted to monotonic testing (Fig. 10) were characterized by large amounts of dimples or microscopic voids, which are typical features of ductile fractures in Al-Mg alloys [29]. The TWB failure occurred in the thinner base material, and since there was little constraint, the fracture essentially proceeded under conditions of plane stress, leading to a complete slant fracture with a plane of maximum shear stress at 45° [30]. It could be seen that the dimples were oriented towards the shear stress direction (Fig. 10(a)). Various shapes of second-phase particles could be observed inside the voids (Fig. 10(b)).
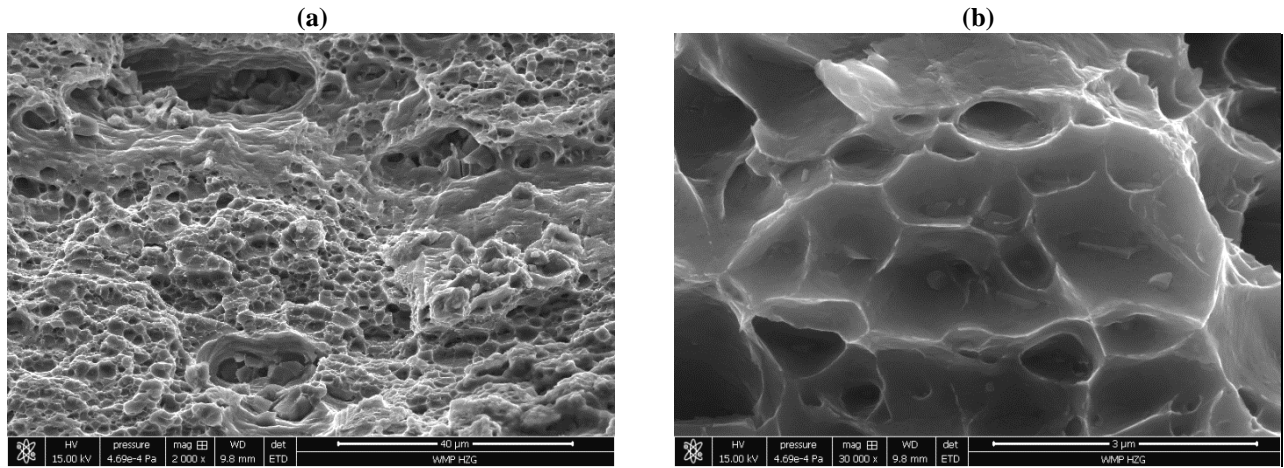
(a)　　　　　　　　　　　　　　　　　　　　(b)

Figure 10: Ductile fracture surface of the TWB joint by SEM macrograph analysis after quasi-static loading test (a) and dimples detail with high magnification (b).

The specimens tested under cyclic loading showed at least three different fracture zones. The crack initiation site is illustrated in Fig. 11(a) for the specimen tested at 50% yield strength. Due to the low stress level, this specimen features a single crack initiation site, and the river marks pattern indicates the direction of crack growth. Fig. 11(b) shows a stable crack propagation regime that is characterised by parallel fatigue patches containing fine striations, which are shown in detail in Fig. 12(a). Each fatigue striation was formed by one loading cycle, so the crack growth rate could be estimated from the spacing between striations. However, the exact location where the striations are measured must be carefully identified, since load variation during slow crack growth can affect the growth rate [30]. Although intergranular crack propagation was identified as the predominant crack growth micromechanism, localized regions of the fracture surface showed brittle fracture, characterized by a pure transgranular cracking propagation (Fig. 12(b)). The region of fast crack growth was characterized by a very ductile fracture with large amounts of varied shape dimples spread out on the surface (Fig. 13).
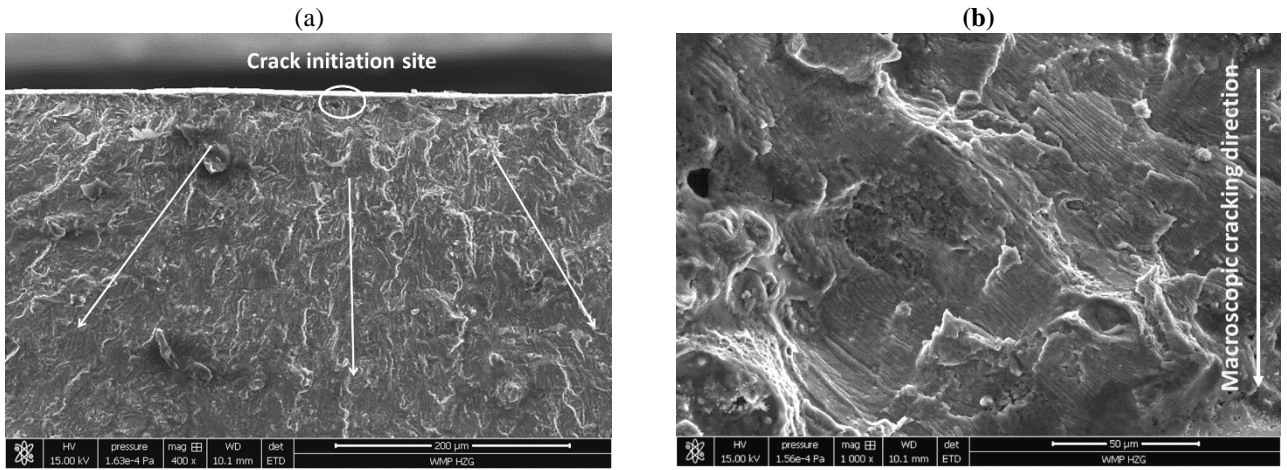
13

Figure 11: SEM micrographs showing the fatigue initiation sites (a) and fatigue crack propagation zone (b).
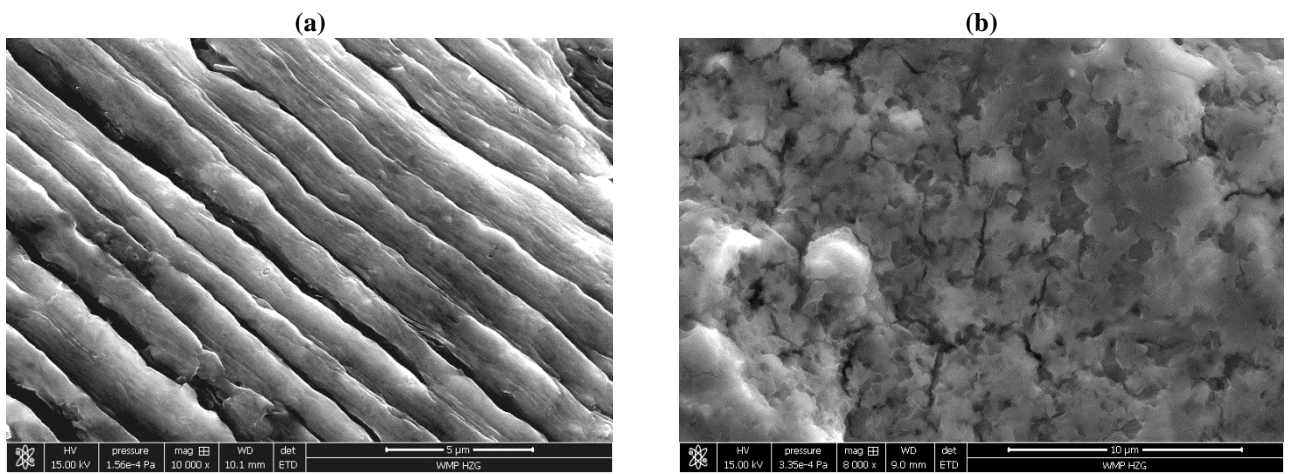

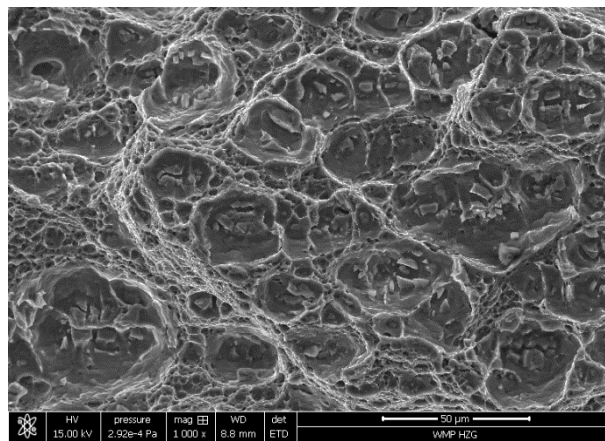Figure 12: Fatigue striations (a) and morphology of the region of fast crack growth (b).

Figure 13: Low magnification view of a fast crack growth region.

4. Conclusions

In the present study, defect-free TWB joints were produced by FSW from dissimilar cold rolled AA5059 and AA5083 Al alloys with thicknesses of 6 and 8 mm, respectively. The following conclusions can be drawn from the results of the analysis and characterisation programme:

- The FSW process altered the central portion (SZ) of the dissimilar TWB, which was completely replaced by a refined microstructure with equiaxed, recrystallized fine grains, producing an overmatch stir zone, as indicated by the microhardness tests.
- Due to the stress concentration factor induced by the geometry of the joints, as well as the overmatch strength in the central portion of the joints, the TWB failure under quasi-static loading took place in the thinner sheet, and the overall mechanical properties of the TWB joints were approximately the same as those of the AA5059 base material used as the thinner sheet.
- Changes in mechanical properties on the local scale were successfully assessed by DIC, and stress-strain curves were calculated for different weld regions. The results suggested that due to the mismatch of mechanical properties and geometric characteristics in the TWB joints, local constraints can impose premature strain in the HAZ zone of the 6mm thickness sheet.
- Fatigue testing of the TWB specimens reached the fatigue limit with a maximum test load of 78MPa. The estimated fatigue class (FAT) of the TWB joint, considering the 95% confidence interval, was 56MPa.
- The fracture surface resulting from quasi-static testing was characterized by a ductile fracture with large amounts of dimples. Due to the plane stress condition in the thinner sheet, a slant fracture with plane of maximum shear stress at 45° occurred, and the dimples were oriented towards the shear stress direction. During cyclic loading, the fracture surface was characterized by parallel fatigue patches containing fine ductile striations, and localised regions of the fracture surface presented a pure transgranular aspect.

Acknowledgments

References

[1]   Ferraris S, Volpone L. M. Aluminium Alloys in Third Millennium Shipbuilding: Materials, Technologies, Perspectives. Fifth Int Forum Alum Ships 2005:11–3.

[2]   Sinke J, Iacono C, Zadpoor AA. Tailor made blanks for the aerospace industry. Int J Mater Form 2010;3:849–52.

[3]   Fratini L, Buffa G, Shivpuri R. Improving friction stir welding of blanks of different thicknesses. Mater Sci Eng 2007;459:209–15.

[4]   Buffa G, Fratini L, Hua J, Shivpuri R. Friction Stir Welding of Tailored Blanks: Investigation on Process Feasibility. CIRP Ann - Manuf Technol 2006;55:279–82.

[5]   Zadpoor AA, Sinke J, Benedictus R, Pieters R. Mechanical properties and microstructure of friction stir welded tailor-made blanks. Mater Sci Eng 2008;494:281–90.

[6]   Zadpoor AA, Sinke J, Benedictus R. Global and Local Mechanical Properties and Microstructure of Friction Stir Welds with Dissimilar Materials and/or Thicknesses. Met Mater Trans 2010;41:3365–78.

[7]   Leitão C, Emílio B, Chaparro BM, Rodrigues DM. Formability of similar and dissimilar friction stir welded AA 5182-H111 and AA 6016-T4 tailored blanks. Mater Des 2009;30:3235–42.

[8]   Lee W, Chung K-H, Kim D, Kim J, Kim C, Okamoto K, et al. Experimental and numerical study on formability of friction stir welded TWB sheets based on hemispherical dome stretch tests. Int J Plast 2009;25:1626–54.

[9]   Chung K, Lee W, Kim D, Kim J, Chung K-H, Kim C, et al. Macro-performance evaluation of friction stir welded automotive tailor-welded blank sheets: Part I – Material properties. Int J Solids Struct 2010;47:1048–62.

[10] Kim D, Lee W, Kim J, Chung K-H, Kim C, Okamoto K, et al. Macro-performance evaluation of friction stir welded automotive tailor-welded blank sheets: Part II – Formability. Int J Solids Struct 2010;47:1063–81.

[11] Garware M, Kridli GT, Mallick PK. Tensile and Fatigue Behavior of Friction-Stir Welded Tailor-Welded Blank of Aluminum Alloy 5754. J Mater Eng Perform 2010;19:1161–71.

[12] Reynolds AP, Duvall F. Digital Image Correlation for Determination of Weld and Base Metal Constitutive Behavior. Weld Res Suppl 1999;355–60.

[13] Leitão C, Galvão I, Leal RM, Rodrigues DM. Determination of local constitutive properties of aluminium friction stir welds using digital image correlation. Mater Des 2012;33:69–74.

[14] Lockwood WD, Reynolds AP. Simulation of the global response of a friction stir weld using local constitutive behavior. Mater Sci Eng 2003;339:35–42.

[15] Leitão C, Costa MI, Khanijomdi K, Rodrigues DM. Assessing strength and local plastic behaviour of welds by shear testing. Mater Des 2013;51:968–74.

[16] ASM International Handbook Committee. ASTM Handbook - Volume 2. Properties and Selection: Nonferrous Alloy and Special-Purpose Materials. Printed in the United States of America; 1992

[17] Nandan R, DebRoy T, Bhadeshia HKDH. Recent advances in friction-stir welding – Process, weldment structure and properties. Prog Mater Sci 2008;53:980–1023.

[18] Von Strombeck A, Sheikhi S, dos Santos JF. Effect of Welding Speed on the Properties of Friction Stir Welded Tailored Blanks. 4th Int. Symp. Frict. Stir Weld., Park City, Utah, USA, 2003.

[19] Sheikhi S, dos Santos JF. On the Formability of Friction Stir Welded Aluminium Tailored Welded Blanks. Proc. Int. Symp. Frict. Stir Weld, 2004.

[20] Mishra RS, Ma ZY. Friction stir welding and processing. Mater Sci Eng R Reports 2005;50:1–78.

[21] Peel M, Steuwer A, Preuss M, Withers PJ. Microstructure, mechanical properties and residual stresses as a function of welding speed in aluminium AA5083 friction stir welds. Acta Mater 2003;51:4791–801.

[22] Rao D, Huber K, Heerens J, dos Santos JF, Huber N. Asymmetric mechanical properties and tensile behaviour prediction of aluminium alloy 5083 friction stir welding joints. Mater Sci Eng 2013;565:44–50.

[23] Riahi M, Amini A. Effect of different combinations of tailor-welded blank coupled with change in weld location on mechanical properties by laser welding. Int J Adv Manuf Technol 2013;67:1937–45.

[24] Korouyeh RS, Naeini HM, Liaghat GH, Kasaei MM. Investigation of Weld Line Movement in Tailor Welded Blank Forming. Adv Mater Res 2012;445:39–44.

[25] Dieter GE. Mechanical metallurgy. 3th ed. New York: McGraw-Hill; 1986.

[26] Reed JM, Walter ME. Observations of serration characteristics and acoustic emission during serrated flow of an Al–Mg alloy. Mater Sci Eng 2003;359:1–10.

[27] ARAMIS GOM: User Manual - Software. Cited 2014 Feb 17. Available from: http://www.gom.com/metrology-systems/system-overview/aramis.html.

[28] Hobbacher A. Recommendations for fatigue design of welded joints and components. Welding Research Council; 2009.

[29] Menzemer C, Srivatsan T. The quasi-static fracture behavior of aluminum alloy 5083. Mater Lett 1999;38:317–20.

[30] ASM International Handbook Committee. ASM Handbook Volume 19: Fatigue and Fracture. Printed in the United States of America; 1996.